Performance Evaluation of VDFLL Architecture for a Dual Constellation L1/E1 GNSS Receiver in Challenging Environments

Enik Shytermeja, Axel Javier Garcia Peña, Olivier Julien

Performance evaluation of VDFLL architecture for a dual constellation L1/E1 GNSS receiver in challenging environments

Enik Shytermeja, Axel Garcia-Pena and Olivier Julien
SIGnal processing and NAVigation (SIGNAV) research group
TELECOM Laboratory
Ecole Nationale de l'Aviation Civile (ENAC)

BIOGRAPHY (IES)

Enik Shytermeja is a PhD researcher within the SIGnal processing and NAVigation (SIGNAV) research group of the TELECOM lab of ENAC (French Civil Aviation University), in Toulouse, France. He received his master degree in telecommunication engineering in 2011 from the Polytechnic University of Tirana in Albania and his 2nd level master degree in "Navigation and Related Applications" with excellent results in 2012 from Polytechnic University of Turin. His research interests are GNSS signal processing and receiver design, GNSS/INS/video hybridization algorithms and integrity monitoring in urban environment.

Axel Garcia Pena is a researcher/lecturer with the SIGnal processing and NAVigation (SIGNAV) research group of the TELECOM lab of ENAC (French Civil Aviation University), Toulouse, France. His research interests are GNSS navigation message demodulation, optimization and design, GNSS receiver design and GNSS satellite payload. He received his double engineer degree in 2006 in digital communications from SUPAERO and UPC, and his PhD in 2010 from the Department of Mathematics, Computer Science and Telecommunications of the INPT (Polytechnic National Institute of Toulouse), France.

Olivier Julien is the head of the SIGnal processing and NAVigation (SIGNAV) research group of the TELECOM lab of ENAC (French Civil Aviation University), Toulouse, France. His research interests are GNSS receiver design, GNSS multipath and interference mitigation, and interoperability. He received his engineer degree in 2001 in digital communications from ENAC and his PhD in 2005 from the Department of Geomatics Engineering of the University of Calgary, Canada.

ABSTRACT

In urban environments, standalone GNSS receivers can be strongly affected to the point of not being able to provide a position accuracy suitable for use in vehicular applications. In this paper, a vector delay/frequency-locked loop (VDFLL) architecture for a dual constellation L1/E1 GPS/Galileo receiver is proposed. In the proposed vectorized architecture, the individual DLLs and FLLs of each tracked satellite are replaced with an Extended Kalman filter (EKF), responsible for both estimating the user's position, velocity and clock bias and closing the code/carrier updates for each GPS L1 and Galileo E1 tracking channels. In this work, a detailed performance comparison between the scalar tracking and VDFLL configuration is assessed under multipath conditions that are generated by the DLR urban multipath channel model. Contrary to the conventional tracking, the L1/E1 VDFLL loop is able to accurately pursue the frequency and code-delay estimation without the requirement of signal reacquisition process and within limited positioning error.

INTRODUCTION

In the last decade, Global Navigation Satellites Systems (GNSS) have gained a significant position in the development of Urban Navigation applications and associated services. A major concern of the constant growth of GNSS-based urban applications is related to the quality of the positioning service, expressed in terms of accuracy, availability and continuity of service but also of integrity provision, ensuring that the application requirements are met [1]. In urban environments, standalone GNSS receiver architectures can be strongly affected to the point of not being able to provide a position accuracy suitable for use in vehicular applications. Specifically, the reception of GNSS signals is affected by the surrounding objects, such as high buildings, trees, lampposts and so on, which can block, shadow, reflect and diffract the received signal. As a result, two significant signal distortions are generated.

On one hand, the reception of reflected or diffracted GNSS LOS echoes in addition to the direct LOS signal generates the phenomenon known as multipath. Multipath echoes represent one of the most detrimental positioning error sources in urban canyons. In fact, the reception of echoes

distorts the ideal correlation function and leads to a degradation of the signal code and carrier estimations accuracy up to a loss of lock of the code and carrier tracking loops. Consequently, the pseudo-range and Doppler measurements are degraded.

On the other hand, the total or partial obstruction of the GNSS LOS by the urban environment obstacles causes GNSS LOS blockage or GNSS LOS shadowing phenomena. The reception of Non-LOS (NLOS) signals due to GNSS LOS signal blockage can then introduce a bias on the pseudo-range measurements if only NLOS satellites are tracked. This bias can be very important as it is representative of the extra-path travelled by the NLOS signal compared to the theoretical LOS signal. The LOS shadowing can also decrease the LOS signal C/N_0 and thus makes the signal more vulnerable to the multipath effects. Finally, the resulting degraded measurements cause the navigation processor to compute an inaccurate position solution or even to be unable to compute one in the case of few available measurements. Therefore, advanced GNSS signal processing techniques must be implemented in order to improve the navigation solution performance in urban environments.

Conventional GNSS receivers basically consist of two units such as, the signal processing module that performs the signal acquisition and tracking tasks for both the code delay and carrier frequency/phase offset and secondly, the navigation module providing the user navigation solution and clock terms estimation. Moreover, in scalar tracking configuration in the presence of weak signals or significant signal power drops, loss of lock of the affected satellite tracking loops occurs and therefore, its estimated pseudoranges are not passed to the navigation processor due to their lack of accuracy.

A promising approach for reducing the effect of multipath interference and NLOS reception is vector tracking (VT), first introduced in [2] where the signal tracking and navigation solution tasks are accomplished by the central navigation filter. In comparison to conventional or scalar tracking (ST), where each visible satellite channel is being tracked individually and independently, VT performs a joint signal tracking of all the satellite channels. Vector tracking exploits the knowledge of the estimated receiver's position and velocity to control the receiver's tracking feedback. In [2], the Vector Delay Lock Loop (VDLL) architecture is explained in details, for which the navigation filter replaces part of the classical delay lock loops (DLLs) structure with an Extended Kalman filter (EKF). In this configuration, the navigation solution drives the code Numerical Control Oscillator (NCOs) of each tracking channel while the carrier frequency/phase estimation is still achieved scalarly by the Frequency or Phase Lock Loops (FLLs or PLLs). Vector DLL (VDLL) tracking performance of the GPS L1 signal in weak signal-to-noise ratio (SNR) environment and robustness against signal interference and attenuation has been demonstrated in [3], [4] and [5].

The objective of this work is to assess the performance of the Vector Delay Frequency Lock Loop (VDFLL) architecture, seen as a combination of the Vectorized DLL (VDLL) and Vectorized FLL (VFLL) loops, in signal-constrained environment. From the navigation point of view, VDFLL represents a concrete application of information fusion, since all the tracking channels Numerical Control Oscillators (NCOs) are controlled by the same navigation solution filter.

In this paper, a dual constellation GPS + Galileo single frequency L1/E1 VDFLL architecture is presented since this type of receiver can significantly improve the availability of a navigation solution in urban canyons and heavily shadowed areas: an increased number of satellites satellite in-view is directly translated in a higher measurement redundancy and improved position reliability. A detailed performance comparison between the scalar tracking and VDFLL configuration in terms of position and code/carrier tracking accuracies is assessed in a urban environment generated using the wideband DLR model [10]. In specifics, this model generates an artificial scenario representing the characteristics of a given urban environment, where the LOS and multipath echoes are generated per each tracked satellite-user propagation channel.

This paper is organized as follows: Section I describes in detail the state and observation model of the proposed dual-constellation single-frequency L1/E1 GPS/Galileo VDFLL algorithm. Section II, providing the Kalman filter measurement generation process, is split in two main parts: Firstly, a short overview of the DLR urban channel propagation model is given with an emphasis on its output vector including the LOS and multipath echoes parameters. Whereas, the second part is dedicated to the mathematical formulation of the multipath-affected correlator outputs that are further employed for the generation of the discriminator outputs. Section III, provides the flowchart of the VDFLL navigation filter, focusing on the measurement prediction and the computation of the observation matrix. The measurement innovation formulation and the VDFLL code and carrier feedback loop model is detailed in Section IV. The simulation test description and the test results, in terms of position/velocity accuracies and EKF estimation errors, are given in Section V. The main conclusions of this paper and future work will be drawn in Section VI.

PROPOSED L1/E1 VDFLL ARCHITECTURE

The proposed VDFLL architecture comprises three sub-modules: the code/carrier tracking loops including the DLL/FLL discriminators, the EKF navigation filter and the code/carrier NCOs update. In this work, we present the dual constellation single frequency band L1/E1 VDFLL architecture, wherein the code (DLL) and frequency (FLL) tracking loops are coupled through the navigation solution computed by the central extended Kalman filter (EKF). The detailed architecture of the proposed L1/E1 VDFLL configuration is sketched in Figure 1.
Kalman filter estimation equations fall into two groups:

- *Time update (Prediction)* equations, performing the forward projection in time of the current vector state $X_k^+ \rightarrow X_{k+1}^-$ and of the state error covariance matrix $P_k^+ \rightarrow P_{k+1}^-$, to provide "*a priori*" estimates for the next time epoch, *k+1*, where *k* indicates the current time epoch;

- *Measurement update (Correction)* equations, responsible for the state vector and state covariance matrix updates that are achieved by feeding the current epoch measurement vector, denoted as z_{input} into the *a priori* estimate, X_{k+1}^- and P_{k+1}^-, to obtain an improved *a posteriori* estimate, X_{k+1}^+ and P_{k+1}^+.

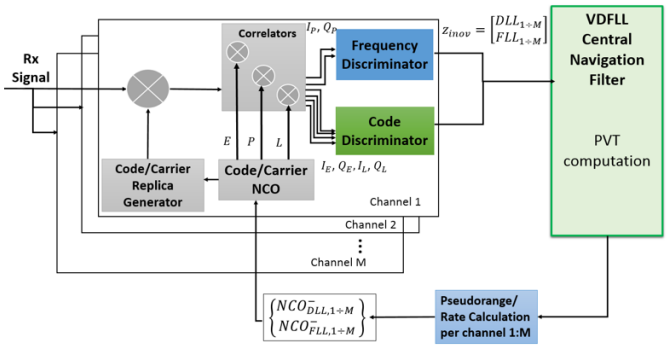

Figure 1. The proposed L1/E1 VDFLL architecture.

EKF State model

The chosen state vector model in our EKF navigation filter implementation is the Position and Velocity (PV) representation, containing the following states:

$$X_k = [x\ \dot{x}\ y\ \dot{y}\ z\ \dot{z}\ \ c \cdot t_{GPS-clk}\ c \cdot t_{GAL-clk} \cdots \\ \cdots c \cdot \dot{t}_{GPS-clk}\ \ c \cdot \dot{t}_{GAL-clk}]_k^T \quad (1)$$

being a 10x1 absolute state vector, containing both the receiver's position vector $[x(k), y(k), z(k)]^T$ and the receiver's velocity vector $[\dot{x}(k), \dot{y}(k), \dot{z}(k)]^T$ in ECEF coordinates; the receiver's clock dynamics comprising the receiver clock bias and drift w.r.t the GPS and Galileo time and drift components $[c \cdot t_{GPS-clk}\ c \cdot t_{GAL-clk}\ c \cdot \dot{t}_{GPS-clk}\ c \cdot \dot{t}_{GAL-clk}]^T$, where c is the speed of light and therefore the clock biases and drift are expressed in unit of [m] and [m/s], respectively.
The system model of the EKF filter in the continuous time domain may be expressed as:

$$\dot{X}(t) = \ \varphi \cdot X(t) + B \cdot w(t), \quad (2a)$$

Where $\dot{X}(t)$ denotes the derivative of the state vector $X(t)$, $w(t)$ is the centered gaussian white noise affecting the state vector, φ is the system matrix and B is the colored noise transition matrix, both in the continuous time domain. Passing to the discrete time domain, the system or dynamic model of the VDFLL navigation filter can be detailed as follows:

$$X_k = \ \Phi \cdot X_{k-1} + w_k, \quad (2b)$$

where: X_k denotes the state vector forward projection from the $k-1^{th}$ to the k^{th} time epoch and Φ represents the dynamics of the user platform and clock, expressed as follows:

$$\Phi = \begin{bmatrix} C & 0_{2\times2} & 0_{2\times2} & 0_{2\times4} \\ 0_{2\times2} & C & 0_{2\times2} & 0_{2\times4} \\ 0_{2\times2} & 0_{2\times2} & C & 0_{2\times4} \\ 0_{4\times2} & 0_{4\times2} & 0_{4\times2} & C_{clk} \end{bmatrix}_{10\times10}, \quad (3)$$

where:

$$C = \begin{bmatrix} 1 & \Delta T \\ 0 & 1 \end{bmatrix} \text{ and } C_{clk} = \begin{bmatrix} 1 & 0 & \Delta T & 0 \\ 0 & 1 & 0 & \Delta T \\ 0 & 0 & 1 & 0 \\ 0 & 0 & 0 & 1 \end{bmatrix} \quad (4)$$

and ΔTdenotes the time interval between two consecutive estimations, representing the measurement update time of the central filter.
The discrete process noise vector w_k is modeled as a Gaussian noise vector with zero mean and discrete covariance matrix Q_k. The process noise w_k comes from two sources namely, the user dynamic noise $[w_x, w_{\dot{x}}, w_y, w_{\dot{y}}, w_z, w_{\dot{z}}]$ (constituted by the user's position and velocity terms) and the receiver's clock noise (local oscillator NCO noise) $[w_b, w_d]$, grouped in a single vector representation as:

$$w_k = [w_x\ w_{\dot{x}}\ w_y\ w_{\dot{y}}\ w_z\ w_{\dot{z}}\ w_{b-GPS}\ w_{b-GAL} \cdots \\ \cdots w_{d-GPS}\ w_{d-GAL}]_k^T \quad (5)$$

In Kalman filtering, the process and the measurement noise covariance matrices are very crucial parameters that significantly affect the performance of the filter. Therefore, an accurate tuning is required to fasten the EKF estimation convergence toward the true user state. The discrete-time process noise covariance matrix Q_k is generated from the continuous-domain process noise Q matrix that represents

the uncertainty of the user's dynamics. It is modelled starting from the continuous time domain noise vector w, based on the influence of five process noise power spectral densities (PSDs) as:

$$Q = E\{w \cdot w^T\} = \text{diag}(\sigma_{\dot{x}}^2, \sigma_{\dot{y}}^2, \sigma_{\dot{z}}^2, \sigma_{b-GPS}^2, \sigma_{b-GAL}^2, \sigma_{d-GPS}^2, \sigma_{d-GAL}^2) \quad (6)$$

Based on their nature, the five tuning factors of process noise Q covariance matrix can be grouped in two main categories, such as:

- *User's dynamics sensitive*: including the velocity error variance terms along the ECEF axes $\left(\sigma_{\dot{x}}^2, \sigma_{\dot{y}}^2, \sigma_{\dot{z}}^2\right)$ that will be projected in the position domain through the state transition matrix Φ and the coloured noise transition matrix B from Eq. (2a).

- *Receiver's oscillator noise PSDs*: including the oscillator's phase noise PSD, σ_b, and the oscillator's frequency noise PSD, σ_d, which by themselves depend on the Allan variance parameters h_0 and h_{-2}.

The process noise covariance matrix $Q_k = diag\ [Q_{x,k}, Q_{y,k}, Q_{z,k}, Q_{c,k}]$ in the discrete domain per each entry can be expressed as:

$$Q_{x,k} = \int_{t_{k-1}}^{t_{k-1}+\Delta T} \Phi_x(\mathrm{T}) \cdot \mathrm{Q}_x \cdot {\Phi_x}^{\mathrm{T}}(\mathrm{T}) \quad (7)$$

where Q_x represents the process noise covariance matrix in the continuous time domain for the user's position and velocity along the x axes. Thus, the user's dynamics process noise discretization for the position- and velocity-states along the x-axes is computed as:

$$Q_{x,k} = \int_{t_{k-1}}^{t_{k-1}+\Delta T} \begin{bmatrix} 1 & \Delta T \\ 0 & 1 \end{bmatrix} \cdot \begin{bmatrix} 0 & 0 \\ 0 & \sigma_{\dot{x}}^2 \end{bmatrix} \cdot \begin{bmatrix} 1 & 0 \\ \Delta T & 1 \end{bmatrix} \quad (8)$$

Finally:

$$Q_{x,k} = \sigma_{\dot{x}}^2 \cdot \begin{bmatrix} {\Delta T^3}/{3} & {\Delta T^2}/{2} \\ {\Delta T^2}/{2} & \Delta T \end{bmatrix} \quad (9)$$

Similarly, the same logic is applied to obtain the discrete-time process noise covariance matrix for the y- and z-axes user's position projections:

$$Q_{y,k} = \sigma_{\dot{y}}^2 \cdot \begin{bmatrix} {\Delta T^3}/{3} & {\Delta T^2}/{2} \\ {\Delta T^2}/{2} & \Delta T \end{bmatrix}, \quad (10)$$

and,

$$Q_{z,k} = \sigma_{\dot{z}}^2 \cdot \begin{bmatrix} {\Delta T^3}/{3} & {\Delta T^2}/{2} \\ {\Delta T^2}/{2} & \Delta T \end{bmatrix} \quad (11)$$

The receiver's clock noise covariance matrix is equal to:

$$Q_{c,k} = \begin{bmatrix} a_{GPS} & 0 & b_{GPS} & 0 \\ 0 & a_{GAL} & 0 & b_{GAL} \\ 0 & 0 & b_{GPS} & 0 \\ 0 & 0 & 0 & b_{GAL} \end{bmatrix}, \quad (12)$$

where:

$$\begin{aligned} a_{GPS} &= \sigma_{b-GPS}^2 \cdot \Delta T + \sigma_{d-GPS}^2 \cdot \frac{\Delta T^3}{3} \\ a_{GAL} &= \sigma_{b-GAL}^2 \cdot \Delta T + \sigma_{d-GAL}^2 \cdot \frac{\Delta T^3}{3} \\ b_{GPS} &= \sigma_{d-GPS}^2 \cdot \frac{\Delta T^2}{2} \\ b_{GAL} &= \sigma_{d-GAL}^2 \cdot \frac{\Delta T^2}{2} \end{aligned} \quad (13)$$

EKF Measurement model

The non-linear relation between the state and the measurement vector is expressed as follows:

$$z_k = h(X_k) + v_k, \quad (14)$$

where h is the *non-linear* function relating the measurement z_k to the state X_k and v_k is *the measurement noise vector* that is modelled as a zero-mean uncorrelated Gaussian noise process and independent to the process noise w_k. The measurement vector z_k comprises the pseudoranges ρ_j and Doppler measurements $\dot{\rho}_j$, output from the code/carrier tracking process for the $j = 1 \div M$ L1/E1 tracking channels:

$$\begin{aligned} z_k = [&h_{sat1}(X_k), \dots, h_{satM}(X_k) \\ &\vdots f_{sat1}(X_k), \dots, f_{satM}(X_k)] \\ = &\left[\left(\rho_1, \rho_2, \cdots, \rho_j\right) \vdots \left(\dot{\rho}_1, \dot{\rho}_2, \cdots, \dot{\rho}_j\right)\right]_k \end{aligned} \quad (15)$$

In the Cartesian ECEF-frame implementation, the pseudoranges $\rho_{j,k}$ per each tracked satellite j are modelled as:

$$\begin{aligned} \rho_{j,k} = h_{satj}(X_k) = &\\ \sqrt[2]{\left(x_{sat\ j,k} - X_k(1)\right)^2 + \left(y_{sat\ j,K} - X_k(3)\right)^2 \cdots} &\\ \sqrt[2]{\cdots + \left(z_{sat\ j,k} - X_k(5)\right)^2} + X_k(7)\ \ (or\ X_k(8)) &\\ + n_{\rho_{j,k}} & \end{aligned} \quad (16)$$

where $R_j(X_k) = \sqrt[2]{\left(x_{sat\ j,k} - X_k(1)\right)^2 + \left(y_{sat\ j,K} - X_k(3)\right)^2 \cdots}$

$\cdots + \sqrt[2]{\cdots + (z_{sat\ j,k} - X_k(5))^2}$ denotes the geometric distance from satellite j to the user at time epoch k.
While the remaining M-entries of the measurement vector, constituted by the Doppler measurements, are modelled as:

$$\begin{aligned}\dot{\rho}_{j,k} = f_{satj}\left(\dot{x}_{sat\ j,k} - X_k(2)\right)\cdot\ a_{x,j} + \cdots \\ \cdots + \left(\dot{y}_{sat\ j,k} - X_k(4)\right)\cdot a_{y,j} + \cdots \\ \cdots + \left(\dot{z}_{sat\ j,k} - X_k(6)\right)\cdot\ a_{z,j} + X_k(9\ or\ 10) + n_{\dot{\rho}_{j,k}},\end{aligned} \tag{17}$$

Where the choice between the 9th or 10th clock drift terms is only related to the GPS or Galileo satellite being tracked, respectively and $(a_{x,j}, a_{y,j}, a_{z,j})$ the a-terms denote the line-of-sight (LOS) unit vectors from the receiver to the j^{th} satellite along the X, Y and Z axes, expressed as:

$$a_{x,j} = \frac{\left(x_{sat\ j,k} - X_k(1)\right)}{R_{j,k}}$$

$$a_{y,j} = \frac{\left(y_{sat\ j,k} - X_k(3)\right)}{R_{j,k}} \tag{18}$$

$$a_{z,j} = \frac{\left(z_{sat\ j,k} - X_k(5)\right)}{R_{j,k}}$$

and $(n_{\rho_{j,k}}, n_{\dot{\rho}_{j,k}})$ denote the zero-mean Gaussian-distributed noise affecting the pseudorange and Doppler measurements, respectively.

The measurement noise vector v_k is modelled as a zero-mean uncorrelated Gaussian noise process and independent to the process noise w_k:

$$E[v_k] = 0 \tag{19}$$

$$E[v_k \cdot w_l^T] = 0 \tag{20}$$

$$E[v_k \cdot v_l^T] = R_k \cdot \delta_{kl}, \text{ for all } k \text{ and } n \tag{21}$$

where $\boldsymbol{\delta_{kl}}$ denotes the Kronecker's delta, and $\boldsymbol{R_k}$ is the *measurement noise covariance matrix*.
In our vector tracking algorithm, the measurements are created by adding the discriminator outputs to the measurement prediction. Assuming that the code delay and carrier frequency errors are small enough to fall into the discriminator linear region, the measurement noise will indeed be represented by the discriminators noise prior to closing the feedback loop of a classical tracking loop, expressed as the open-loop noise configuration.
The measurement noise covariance matrix has in the main diagonal the following entries:

$$R_{jj} = \begin{cases}\sigma^2_{Code\_Discri,j} & for \quad j = 1 \cdots M \\ \sigma^2_{Carr-Discri,j} & for \quad j = 1 \cdots M\end{cases} \tag{22}$$

where the first entry refers to the pseudorange error variance terms for the tracked GPS and Galileo satellites, while the second one is a common term for the pseudorange rate error variance for all tracked satellites.

MEASUREMENT GENERATION PROCESS

In the tracking stage, the generation of the correlator outputs is certainly affected by the LOS and multipath echoes amplitude, delay and phase that furthermore increase the code delay and carrier frequency estimation errors. For a clearer understanding of the measurement generation process, a short description of the DLR urban multipath model will be given.

DLR Multipath model: Inputs/Outputs

The DLR Land Mobile Multipath Channel Model (LMMC) was developed thanks to an extensive measurement campaign conducted by DLR in 2002 and is a freely accessible model for academic purposes that can be downloaded from the DLR website[10], [11]. This model generates an artificial scenario having the urban environment characteristic including potential obstacles to the received GNSS signal such as trees, buildings, lampposts and reflectors as given in Figure 2. These obstacles are statistically generated but the amplitude, the phase and the delay associated to the LOS and multipath components are mainly deterministically determined by ray tracing and geometric techniques. Moreover, the number of echoes and their life span are statistical variables depending on the satellite elevation angle. The main inputs of this model are the urban scenario characteristic (including the road width, building height etc), the receiver speed and heading angle, the satellite elevation and azimuth angles in degrees.

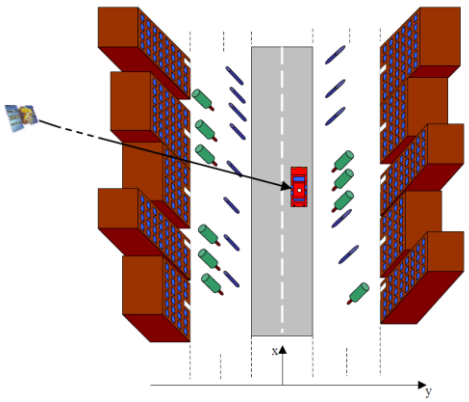

Figure 2. Artificial urban scenario generated by the DLR urban propogation channel model [10].

Multipath-affected correlator outputs

In order to obtain a realistic vehicle urban scenario coherent with the reference car trajectory fed to the EKF

navigation filter, several modification were applied to the DLR model. Firstly, the DLR urban trajectory was generated at a sampling frequency equal to the VDFLL position update rate. Secondly, this model was adapted in such a manner that can provide the amplitude, delay, phase and Doppler frequency of the LOS and multipath echoes as an output vector for each epoch *k*:

$$output_k = \left(A_{LOS}, \tau_{LOS}, \varphi_{LOS}, f_{D_{LOS}}\right)_{i,k}; \cdots \\ \cdots \left(A_{NLOS}, \tau_{NLOS}, \varphi_{NLOS}, f_{D_{NLOS}}\right)_{j,k} \quad (23)$$

Where:

- $\left(A_{LOS}, \tau_{LOS}, \varphi_{LOS}, f_{Dopp_{LOS}}\right)_i$ – the LOS rays ($i = 1 \div nr\_LOS$) amplitude, delay, phase and Doppler freq;
- $\left(A_{NLOS}, \tau_{NLOS}, \varphi_{NLOS}, f_{Dopp_{NLOS}}\right)_j$ –the NLOS rays ($j = 1 \div nr\_NLOS$) amplitude, delay, phase and Doppler freq.

It must be noted that the DLR model provides up to 3 LOS rays, due to the diffraction effects occurring for certain geometries.
Furthermore, the LOS and NLOS echoes information, given above in Eq. (24), is used to generate the correlator outputs in the tracking stage of the VDFLL algorithm per each satellite in view, as follows (for j[th] satellite):

$$\begin{aligned} IX_j = &[\sum_{i=1}^{N_{LOS}} A_{i,LOS} \cdot R\left(\varepsilon_{\tau_{i,LOS}} + p\right) \cdot \cos\left(\varepsilon_{\varphi_{i,LOS}}\right) \\ &\cdots \cdot \operatorname{sinc}\left(\pi \cdot \varepsilon_{f_{D\,i,LOS}} \cdot T_s\right)]_j \\ +[&\sum_{i=1}^{N_{NLOS}} A_{i,NLOS} \cdot R\left(\varepsilon_{\tau_{i,NLOS}} + p\right) + \cos\left(\varepsilon_{\varphi_{i,NLOS}}\right) \\ &\cdots \cdot \operatorname{sinc}\left(\pi \cdot \varepsilon_{f_{D\,i,NLOS}} \cdot T_s\right)]_j + n_{Ij} \\ QX_j = &[\sum_{i=1}^{N_{LOS}} A_{i,LOS} \cdot R\left(\varepsilon_{\tau_{i,LOS}} + p\right) \cdot \sin\left(\varepsilon_{\varphi_{i,LOS}}\right) \\ &\cdots \cdot \operatorname{sinc}\left(\pi \cdot \varepsilon_{f_{D\,i,LOS}} \cdot T_s\right)]_j \\ +[&\sum_{i=1}^{N_{NLOS}} A_{i,NLOS} \cdot R\left(\varepsilon_{\tau_{i,NLOS}} + p\right) \cdot \sin\left(\varepsilon_{\varphi_{i,NLOS}}\right) \\ &\cdots \cdot \operatorname{sinc}\left(\pi \cdot \varepsilon_{f_{D\,i,NLOS}} \cdot T_s\right)]_j + n_{Qj} \end{aligned} \quad (24)$$

Where:

- the p parameter indicates the Early, Prompt and Late code delay depending on the E-L chip spacing T_c , given as :

$$\begin{Bmatrix} p = -T_c/2 & if\ X = Early \\ p = 0 & if\ X = Prompt \\ p = T_c/2 & if\ X = Late \end{Bmatrix}$$

- $\varepsilon_{\tau_{i,LOS/NLOS,j}} = \tau_{LOS/NLOS,i,j} - \tau_{est,VDFLL,j}$ denotes the LOS/NLOS code delay error computed as the difference between the true code delay of the i[th] LOS or i[th] NLOS signal of the j[th] received satellite and the VDFLL estimated one, respectively;
- $\varepsilon_{\varphi_{i,LOS/NLOS,j}} = \varphi_{LOS/NLOS,i,j} - \varphi_{est,VDFLL,j}$ denotes the carrier phase error computed as the difference between the true phase of the i[th] LOS or i[th] NLOS signal of the j[th] received satellite and the VDFLL estimation, respectively;
- $\varepsilon_{f_{D\,i,LOS/NLOS,j}} = f_{D_{LOS/NLOS,i,j}} - f_{D_{est,VDFLL,j}}$ denotes the Doppler frequency error computed as the difference between the true Doppler frequency of the i[th] LOS or i[th] NLOS signal of the j[th] received satellite and its VDFLL estimation, respectively;
- n_{Ij} and n_{Qj} represent the In Phase and Quadrature correlator output noise terms of the j[th] tracked channel, respectively.

EKF Innovation vector

The code delay and frequency carrier estimation process are achieved per channel basis as in the scalar configuration, however in the vectorized architecture, the DLL and FLL discriminator outputs will be directly fed to the EKF navigation filter as its measurement innovation vector.
The state vector estimate update $\boldsymbol{X_k^+}$ is obtained using the following expression:

$$X_k^+ = X_k^- + K_k \cdot \delta z_k \ = X_k^- + K_k \cdot \delta z_k \quad (25)$$

Where δz_k represents the measurement innovation vector, including the pseudorange and pseudorange rate errors for each tracking channel $j = 1 \div M$ that are computed from the DLL and FLL discriminator outputs, is given as:

$$\begin{aligned} z_{innov} &= z_{input} - h(X_k^-) \\ &= (h(X_k^-) + \varepsilon_{discri}) - h(X_k^-) \\ &= [\delta\rho_1, \delta\rho_2 \cdots \delta\rho_M \vdots \delta\dot{\rho}_1, \delta\dot{\rho}_2 \cdots \delta\dot{\rho}_M]_k \end{aligned} \quad (26)$$

where the first M terms, related to the pseudorange errors, are computed from the DLL discriminator outputs using the following relation:

$$\delta z_{\delta\rho|k} = \left[\left(\frac{c}{f_{code}}\right) \cdot \left(D_{DLL,1}, \cdots, D_{DLL,M}\right)\right]_k \quad (27)$$

Similarly, the pseudorange rate errors computation for each channel is achieved from the FLL discriminator outputs:

$$\delta z_{\delta\rho_{\dot{FLL}}|k} = \left[\left(\frac{c}{f_{carr}}\right)\cdot\left(D_{FLL,1},\cdots,D_{FLL,M}\right)\right]_k \quad (28)$$

VDFLL POSITION ESTIMATION WORKFLOW

Following the VDFLL estimation workflow of Figure 3, the successive step after the state propagation or prediction, is the computation of the Kalman gain in Step 2.1. For this matter, the measurement prediction z_k and observation matrix H_k shall be calculated. Afterwards, the state vector update is computed from the measurement innovation vector input to the EKF navigation filter, which comprises the code and carrier discriminator outputs from the tracking loops. Finally, the code and carrier NCO update, computed from the EKF filter prediction states, closes the feedback loop to the tracking module and will be given in details in the last section.

Measurement Prediction

The predicted measurement vector z_k^- consists of two entries per satellite tracking channel, in specifics the predicted pseudorange $\rho_{j,k}^-$ and pseudorange rates $\dot{\rho}_{j,k}^-$:

$$z_k^- = [\,\rho_{1,k}^-,\cdots\,\rho_{M,k}^-,\dot{\rho}_{1,k}^-,\cdots\,\dot{\rho}_{M,k}^-]_{2M\times 1}^T, \quad (29)$$

where M denotes the total nr of tracked GPS + Galileo satellites in the current measurement epoch k.
In the Cartesian ECEF-frame implementation, the predicted satellite-user ranges ${R^-}_{j,k}$ per each tracked satellite j are furtherly computed as:

$$R^-_{j,k} = R_{j,k}(X_k^-) = \sqrt[2]{\left(x_{sat\,j,K} - X_k^-(1)\right)^2 + \left(y_{sat\,j,K} - X_k^-(3)\right)^2\cdots} \sqrt[2]{\cdots + \left(z_{sat\,j,k} - X_k^-(5)\right)^2} \quad (30)$$

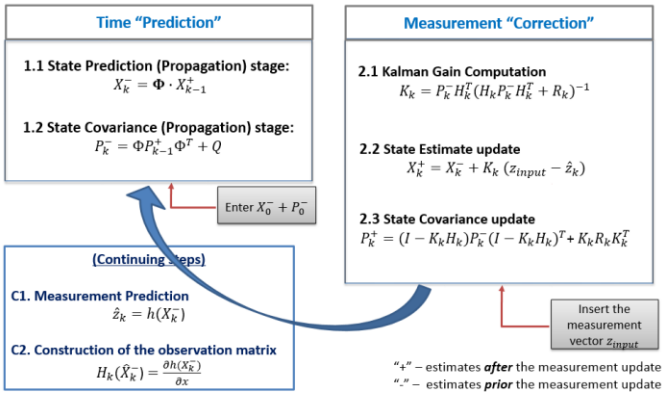

Figure 3. Flowchart of the EKF VDFLL estimation process.

The predicted pseudorange measurement ${\rho^-}_{j,k}$ can be obtained by adding to the predicted distance ${R^-}_{j,k}$, the EKF clock bias estimation $x_k^-(7)$:

$$\begin{aligned} {\rho^-}_{j-GPS,k} &= h_{Sat-GPS,j}(X_k^-) \\ &= {R^-}_{GPSj,k} + X_k^-(7) \\ {\rho^-}_{j-GAL,k} &= h_{Sat-GAL,j}(X_k^-) \\ &= {R^-}_{GALj,k} + X_k^-(8) \end{aligned} \quad (31)$$

where, the first expression denotes the predicted pseudoranges from the GPS satellites comprising the predicted user clock bias w.r.t to GPS time; while the former relation is linked to the Galileo-related predicted ranges.
Similarly, the predicted pseudorange rate ${\dot{\rho}^-}_{j,k}$ can be computed as:

$$\begin{aligned} {\dot{\rho}^-}_{j,k} = f_{sat,j}(X_k^-) = \left(\dot{x}_{sat\,j,k} - X_k^-(2)\right)\cdot a_{x,j}^- + \cdots \\ \cdots + \left(\dot{y}_{sat\,j,k} - X_k^-(4)\right)\cdot a_{y,j}^- + \cdots \\ \cdots + \left(\dot{z}_{sat\,j,k} - X_k^-(6)\right)\cdot a_{z,j}^- + X_k^-(9) \end{aligned} \quad (32)$$

where: $(x_{sat\,j,k}, y_{sat\,j,k}, z_{sat\,j,k})$ and $(\dot{x}_{sat\,j,k}, \dot{y}_{sat\,j,k}, \dot{z}_{sat\,j,k})$ denote the 3D position and velocity vector, respectively, of the j^{th} satellite that are obtained from the ephemerides data and expressed in Cartesian coordinates; while $(X_k^-(1), X_k^-(3), X_k^-(5))$ and $(X_k^-(1), X_k^-(3), X_k^-(5))$ refer to the predicted user's absolute position and velocity vectors along the X, Y and Z axes; while $(X_k^-(7), X_k^-(8))$ are the user's clock predicted bias w.r.t to the GPS and Galileo time and $X_k^-(9)$ denotes the clock drift predictions from the EKF navigation filter.The line-of-sight (LOS) unit vectors from the receiver to the j^{th} satellite along the X, Y and Z axes are computed as follows:

$$a_{x,j}^- = \frac{\left(x_{sat\,j,k} - X_k^-(1)\right)}{{R^-}_{j,k}}$$

$$a_{y,j}^- = \frac{\left(y_{sat\,j,k} - X_k^-(3)\right)}{{R^-}_{j,k}} \quad (33)$$

$$a_{z,j}^- = \frac{\left(z_{sat\,j,k} - X_k^-(5)\right)}{{R^-}_{j,k}}$$

From the pseudorange rate expression, let us denote by $V_{j,k}^-$ the relative satellite-receiver velocities without taking into account the clock drift component as:

$$V_{j,k}^- = \left(\dot{x}_{sat\,j,k} - X_k^-(2)\right)\cdot a_{x,j}^- + \cdots \quad (34)$$

$$\cdots + \left(\dot{y}_{sat\ j,k} - X_k^-(4)\right) \cdot\ a_{y,j}^- + \cdots$$
$$\cdots + \left(\dot{z}_{sat\ j,k} - X_k^-(6)\right) \cdot\ a_{z,j}^-$$

Construction of the measurement matrix R_k

The predicted measurements, incorporated in the predicted measurement vector z_k^-, are communicated to the main EKF filter as a function of the predicted state vector X_k^- through the observation (design) matrix H_k :

$$H_k(X_k^-) = \left.\frac{\partial h(X_k^-)}{\partial X}\right|_{X=X_k^-} \tag{35}$$

The entry (j,m) of the observation matrix $H_k(j,m)$ is the partial derivative w.r.t the predicted position $\partial h_j(X_k^-)/\partial X_m$,where $j = 1 \cdots M$ refers to the M tracking channels and $m = 1 \div 9$ denotes the nine states of the predicted state vector X_k^-.

Let us first compute the 1st row of the design matrix $H_k(j,m)$ that are the partial derivatives of the $H_k(j,m)$ entries related to the predicted pseudorange measurements $\rho^-_{\ j,k}$ w.r.t the predicted state vector elements X_k^-:

$$\left[\frac{\partial h_{Sat-GPSj}(X_k^-)}{\partial X_k^-(1)} \cdots \frac{\partial h_{Sat-GPSj}(X_k^-)}{\partial X_k^-(9)}\right] = \cdots$$
$$\ldots = [-a_{x,j}^-\ 0\ -a_{y,j}^-\ 0\ -a_{z,j}^-\ 0\ 1\ 0\ 1\ 0]^T_{N_{GPS}\times 1}$$

$$\left[\frac{\partial h_{Sat-GALj}(X_k^-)}{\partial X_k^-(1)} \cdots \frac{\partial h_{Sat-GALj}(X_k^-)}{\partial X_k^-(10)}\right] = \cdots \tag{36}$$
$$\ldots = [-a_{x,j}^-\ 0\ -a_{y,j}^-\ 0\ -a_{z,j}^-\ 0\ 0\ 1\ 0\ 1]^T_{(M-N_{GPS})\times 1}$$

where N_{GPS} denotes the number of tracked GPS satellites. The remaining M to 2M rows of the design matrix $H_k(j,m)$ include the partial derivatives of the predicted pseudorange rates measurements $\dot{\rho}^-_{\ j,k}$ w.r.t the predicted state vector X_k^-. The partial derivatives are computed separately for the position and velocity terms of the predicted state vector X_k^-. Regarding the X-position related terms, the following relations can be written:

$$v_{x,j}^- = \frac{\partial f_{satj}(X_k^-)}{\partial X_k^-(1)} = \left(x_{sat\ j,k} - X_k^-(1)\right) \cdot \cdots \cdot \frac{V_{j,k}^-}{{R_{j,k}^-}^2} - \frac{\left(\dot{x}_{sat\ j,k} - X_k^-(2)\right)}{R_{j,k}^-} \tag{37}$$

Similarly, for the partial derivatives of the pseudorange rates w.r.t the predicted user position along the Y and Z-axes, denoted respectively as $X_k^-(3)$ and $X_k^-(5)$:

$$v_{y,j}^- = \frac{\partial f_{satj}(x_k^-)}{\partial X_k^-(3)} = \left(x_{sat\ j,k} - X_k^-(3)\right) \cdot \cdots \cdot \frac{V_{j,k}^-}{{R_{j,k}^-}^2} - \frac{\left(\dot{x}_{sat\ j,k} - X_k^-(4)\right)}{R_{j,k}^-} \tag{38}$$
$$v_{z,j}^- = \frac{\partial f_j(x_k^-)}{\partial X_k^-(5)} = \left(x_{sat\ j,k} - X_k^-(5)\right) \cdot \cdots \cdot \frac{V_{j,k}^-}{{R_{j,k}^-}^2} - \frac{\left(\dot{x}_{sat\ j,k} - X_k^-(6)\right)}{R_{j,k}^-}$$

On the other side, the design matrix $H_k(j,m)$ elements corresponding to the partial derivatives of the predicted pseudorange rates measurements $\dot{\rho}^-_{\ j,k}$ w.r.t the velocity terms of the predicted state vector X_k^-, are computed as follows:

$$v_{\dot{x},j}^- = \frac{\partial f_{satj}(X_k^-)}{\partial X_k^-(2)} = -a_{x,j}^-$$

$$v_{\dot{y},j}^- = \frac{\partial f_{satj}(X_k^-)}{\partial X_k^-(4)} = -a_{y,j}^- \tag{39}$$

$$v_{\dot{z},j}^- = \frac{\partial f_{satj}(X_k^-)}{\partial X_k^-(6)} = -a_{z,j}^-$$

and w.r.t the clock bias drift term x_7 of the predicted state vector X_k^-:

$$v_{c\cdot\dot{t}_{clk},j,k}^- = \frac{\partial h_j\left(\dot{\rho}^-_{\ j,k}\middle| X_k^-\right)}{\partial X_k^-(9)\ or\ \partial X_k^-(10)} = 1 \tag{40}$$

VDFLL FEEDBACK LOOP: CODE AND CARRIER NCO UPDATE

The code and carrier NCO update for the successive time epoch *k+1* is performed per each tracked channel *j* based on the EKF state vector prediction X_k^- from Eq. (4). The pseudorange rate prediction, including the contribution of the satellite clock drift error $\dot{b}_{sv-c,j,k}$, is given by:

$$\begin{aligned}\dot{\rho}^-_{\ j,k+1} = &\left(\dot{x}_{sat\ j,k+1} - X_{k+1}^-(2)\right) \cdot\ a_{x,j}^- + \cdots \\ &\cdots + \left(\dot{y}_{sat\ j,k+1} - X_{k+1}^-(4)\right) \cdot\ a_{y,j}^- + \cdots \\ &\cdots + \left(\dot{z}_{sat\ j,k+1} - X_{k+1}^-(6)\right) \cdot\ a_{z,j}^- + \cdots \\ &\cdots + (X_{k+1}^-(9)|GPS\ or X_{k+1}^-(10)|GAL) + \cdots \\ &\cdots + \dot{b}_{sv-c,j,k+1}\end{aligned} \tag{41}$$

The Doppler frequency correction $\delta f_{D\ j,k+1}^-$ per each tracking channel *j*, closing the feedback loop to the carrier NCO, is computed by projecting the predicted velocity-

and clock drift errors states in the pseudorange rate error domain as:

$$f_{NCO-ca,j,k+1} = \delta f_{D}{}^{-}_{j,k+1} = \frac{f_{carr}}{c} \cdot \dot{\rho}^{-}_{j,k+1} \ (Hz) \qquad (42)$$

where: $f_{carr} = 1{,}57542\ GHz$ refers to GPS L1 & Galileo E1 carrier frequency and $c = 3 \cdot 10^8$ is the speed of light in (m/s).
On the other hand, the code NCO command for each channel j is forwarded to successive tracking epoch by taking the difference between the pseudorange predictions of two consecutive measurement epochs, denoted as $\rho^{-}{}_{j,k+1}$ and $\rho^{-}{}_{j,k}$, respectively:

$$f_{NCO-co,j,k+1} = f_{code} \cdot \frac{(\rho^{-}{}_{j,k+1} - \rho^{-}{}_{j,k})}{c \cdot T_{EKF}} \qquad (43)$$

where T_{EKF} is the EKF update time set to the code and carrier accumulation period.

PERFORMED TESTS

In order to test the performance of the proposed L1/E1 VDFLL architecture, a GNSS emulator compiled in C language, able to generate GPS L1 and Galileo E1 signals up to 48 channels simultaneously, was used. Moreover, the vector tracking algorithm is implemented in C language platform, driven by the faster execution time of KF algorithm at high rates (set equal to the tracking outputs at 50 Hz, $T_{EKF} = 20ms$). Three distinctive GNSS receiver architectures will be analyzed with the scope of performance comparison:

- Scalar tracking employing a 3rd order loop PLL and a DLL, with a KF positioning module at 1 Hz for the PVT computation, where the pseudorange and Doppler measurements are included in the observation vector.

- The same scalar tracking architecture but now integrated with a KF positioning module at 50 Hz, similar to the VDFLL algorithm update rate.

- The proposed VDFLL EKF architecture working at $T_{EKF} = 20ms$ integration time and thus providing 50 Hz code and carrier frequency updates.

It must be noted the KF positioning module is similar to the EKF filter of the vectorized solution, with the differences that a closed-loop measurement covariance matrix is used in the former and moreover, the KF filter operates on locked satellites only whereas the VDFLL uses all satellites in view.

The simulations performed in this work are related to a real car trajectory in Toulouse urban area. The simulated reception conditions are that of a complete urban model integrated to the receiver model, in order to observe the tracking performance of the proposed VDFLL architecture with respect to conventional tracking. In both test scenarios, there is maximum of 7 simultaneously tracked GPS L1 and Galileo E1 channels during 100 GPS epochs. For simplification purposes, the GPS and Galileo reference times are assumed to be perfectly synchronized.
A detailed performance comparison between the scalar and vectorized configurations will be assessed in two different levels:

- *System level*: expressed in terms of user's position and velocity estimation accuracies, position and velocity errors statistics and resistance to degraded signal reception conditions;

- *Channel level*: indicated by the code delay and carrier Doppler frequency estimation errors and their standard deviations in the presence of outages.

In details, the code and carrier tracking parameters used by the scalar configuration and the vectorized architecture are summarized in Table 1.

Table 1. Code and Carrier tracking parameters employed in the scalar and vectorized architectures

L1/E1 Code Tracking Parameters	
DLL order	1
DLL noise bandwidth (B_{DLL-n})	1 Hz
DLL period	0.02 s
Code delay discriminator	Early Minus Late Power (EMLP)
GPS L1 chip spacing (k_{Cs-L1})	0.5 chips
GAL E1 chip spacing (k_{Cs-E1})	0.2 chips
L1/E1 Carrier Tracking Parameters	
Scalar Configuration	
PLL order	3
PLL noise bandwidth (B_{PLl-n})	10 Hz
PLL period	0.02 s
Carrier phase discriminator	Costas Discriminator
Vectorized Architecture	
Carrier frequency period	0.01 s
Carrier frequency discriminator	Cross Dot Product

In the proposed VDFLL architecture, an Early Minus Late Power (EMLP) discriminator has been chosen for both the GPS BPSK and Galileo E1 BOC (1,1) channels. The DLL tracking error variance in presence of thermal noise and in the open-loop configuration, for both GPS L1 and Galileo E1 channels is computed as [8]:

$$\sigma^2_{EMLP-open,j} = \left(\frac{c}{f_{code}}\right)^2 \cdot \left(\frac{C_s}{4 \cdot \alpha \cdot C/N_{0_{est,j}} \cdot T_{DLL}}\right) \cdot \left(1 + \frac{2}{(2 - \alpha \cdot C_s) \cdot C/N_{0_{est,j}} \cdot T_{DLL}}\right) (m^2) \quad (44)$$

The FLL performs the Doppler frequency tracking of the incoming signal that is dominated by the satellite-to-receiver motion and the user clock drift. The FLL tracking error variance of the Decision-Directed cross-product (DDCP) discriminator in the open-loop configuration is given by:

$$\sigma^2_{FLL-open,j} = \left(\frac{c}{f_{carr}}\right)^2 \cdot \left[\frac{1}{\frac{C}{N_{0_{est,j}}} \cdot T^3_{FLL}} \cdot\right] (m^2/s^2), \quad (45)$$

where T_{DLL} and T_{FLL} denote the code and carrier filter integration interval equal to 20 ms; C_s is the code chip spacing (0.5 chips for GPS L1 and 0.2 chips for Gal E1 BOC (1,1); α is a coefficient reflecting the sharpness of the code autocorrelation function (1 for BPSK(1) and 3 for BOC (1,1)); $C/N_{0_{est,j}}$ refers to the estimated carrier-to-noise ratio from the tracking loop of the incoming signal from the $j-th$ tracking channel and $f_{code} = 1.023\ Mhz$ and $f_{carr} = 1.57542\ GHz$ denote the L1/E1 code chipping rate and carrier frequency, respectively.

The simulations herein presented use the GPS and Galileo constellations in the L1 band, taking into consideration the binary phase shift keying BPSK(1) modulation for GPS L1 and the binary offset carrier modulation BOC(1,1) for the pilot signals. As previously stated, the received signals were simulated at the correlator output level in an ENAC-owned semi-analytic receiver simulator. For the scalar tracking architecture, the satellite lock detection test is implemented through the C/N_0 estimator [2] and a hot re-acquisition process of 1 second duration is implemented with initial code errors related to the L1 and E1 code autocorrelation sharpness and initial frequency errors equal to Doppler bin size of 25 Hz. An RF front-end with a 24 MHz bandwidth (double-sided) is assumed.

The oscillator's phase noise PSD σ_b and the oscillator's frequency noise PSD σ_d, which by themselves depend on the Allan variance parameters h_0 and h_{-2} [2], are given as:

$$S_{c\varphi} = \omega_c^2 \cdot \frac{h_0}{2}$$
$$S_{cf} = 2\pi^2 \cdot \omega_c^2 \cdot h_{-2} \quad (46)$$

In our implementation, a Temperature Controlled Oscillator (TCXO) is chosen, where $\omega_c = 2\pi \cdot f_{carr}$ is the carrier frequency expressed in radians and the white noise frequency (h_0) and integrated frequency noise (h_{-2}) have the following values:

$$h_0 = 1 \cdot 10^{-21}$$
$$h_{-2} = 2 \cdot 10^{-20} \quad (47)$$

In the following subsections, the performance comparison between the conventional tracking and the vectorized algorithm will be exploited for the automotive GNSS usage in urban conditions.

Car Trajectory

A realistic car trajectory in high dynamic condition is generated based on the reference trajectory computed by the NovAtel's SPAN receiver mounted on car during a 40 minutes measurement campaign conducted in Toulouse. It must be noted that the simulated car path of 100 seconds duration is a representative of a car trajectory but not of urban signal reception conditions since the simulated received conditions are generated from the DLR urban multipath model. Besides, since the reference trajectory is output at 1 Hz rate, interpolation is used to generate the true trajectory at the VDFLL EKF filter rate @ 50 Hz. The simulated car path is shown in Fig. 4. Moreover, the position domain comparison is extended to the scalar tracking architecture with the KF module working in the same rate as the vectorized architecture at 50 Hz.

Figure 4. The reference trajectory along the city of Toulouse, France.

DLR urban scenario generation

The urban environment conditions are generated for each GPS and Galileo tracked satellite by feeding their elevation and azimuth angles to the modified DLR urban channel. In the scenario generation process, the vehicle is set to drive in the middle of the road with the antenna height at 2 m and the building average height set to 10 m, while for coherency issues, the car speed and heading angle is read

from the reference trajectory at a sampling frequency equal to the VDFLL position update. The satellite-user channel impulse response (CIR) representation at a certain time epoch is depicted in Figure 5, where the first subplot indicates the power in dB of the LOS path (in red) and the multipath echoes (in blue) while in the second subplot, their phases in radians are illustrated. For certain time epochs, the only NLOS reception may occur due the total blockage of the LOS signal that cause fast variation of the signal code delay and frequency error estimation up to total signal's loss of lock, as it will be shown in the result later on.

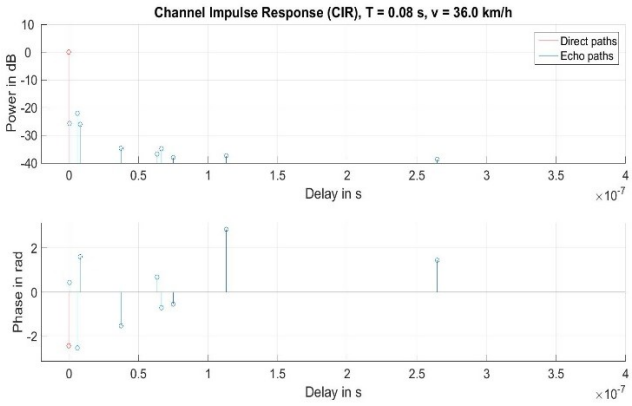

Figure 5. Representative of the satellite channel impulse response (CIR) under multipath reception: **a)** Signal power in dB w.r.t the delay arrival time and **b)** the signal's phase in radians of the LOS ray (in red) and multipath echoes (in blue).

Simulation Results

The positioning root mean square errors (RMSE) per each ECEF axes illustrated in Figure 6, highlight the positioning robustness of the vectorized architecture in the multipath reception conditions. The position and clock bias error statistics for the two scalar configurations and the VDFLL architecture, given in Table 2, provide us interesting results that ought to be analyzed in details.

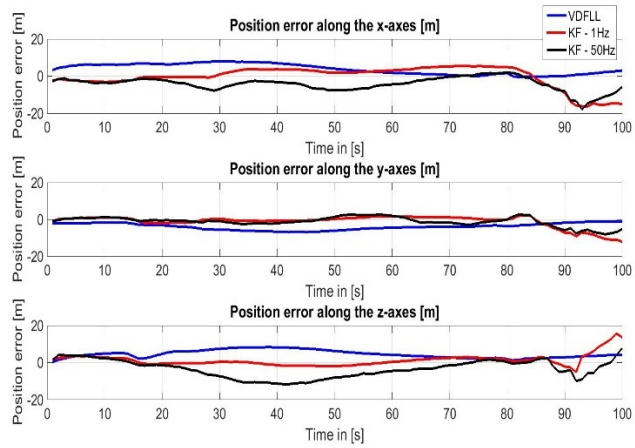

Figure 6. Position error comparison between the scalar tracking + KF positioning module @ 1 Hz (in red), the VDFLL algorithm (in blue) and the scalar tracking + KF positioning module @ 50 Hz (in black) for a car trajectory under multipath reception condition along the: **a)** X-axis in [m]; **b)** Y-axis in [m]; **c)** Z-axis in [m].

Table 2. Position and clock bias error statistics for the scalar tracking + KF position modules @1 Hz and @ 50 Hz and the proposed VDFLL technique prior and after the occurrence of the frequent variation of the number of locked satellites.

	Scalar + KF module @ 1 Hz			
	Prior to the 75th epoch		*After the 75th epoch*	
	E[m]	**Std[m]**	**E[m]**	**Std[m]**
X-error	1.471	2.7	-5.45	8.82
Y-error	0.67	1.06	-4.28	4.76
Z-error	0.51	1.71	3.42	5.01
	Scalar + KF module @ 50 Hz			
	Prior to the 75th epoch		*After the 75th epoch*	
	E[m]	**Std[m]**	**E[m]**	**Std[m]**
X-error	-3.68	2.22	-5.55	6.25
Y-error	-2.4	1.54	-3.25	3.44
Z-error	-4.16	4.76	-3.49	4.24
	VDFLL @ 50 Hz			
	Prior to the 75th epoch		*After the 75th epoch*	
	E[m]	**Std[m]**	**E[m]**	**Std[m]**
X-error	4.79	2.54	0.77	1.01
Y-error	-4.42	1.63	-2.36	0.95
Z-error	5.14	2.07	2.80	0.8
Comment :				
E[] - mean value				
Std[] - standard deviation				

It can be obviously noted that up to 75th time epoch, the position and clock bias error mean and standard deviation of the scalar tracking with the navigation module operating at 1 Hz rate, are significantly lower w.r.t to the other two configurations under test. The reasoning behind this behavior is twofold: On the first place, in the scalar tracking algorithm only the measurements provided by the satellites passing the lock condition test are fed to the navigation filter and secondly, the slower position update rate at 1 Hz assures the KF stability due to a more accurate measurement covariance matrix R_k computation linked to the longer accumulation time. The above given reasoning holds in the case of an overdetermined number of locked satellites that according to Figure 7 d) is valid with seven locked satellites up to the 75th epoch where higher oscillations of the locked satellites are observed.

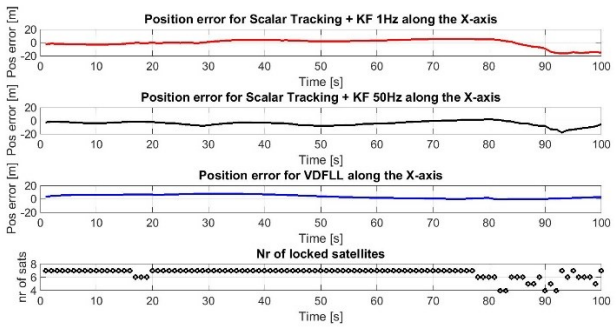

Figure 7. Position error comparison along the X-axis in [m] between: **a)** the scalar tracking + KF positioning module @ 1 Hz (in red), **b)** the scalar tracking + KF positioning module @ 50 Hz (in black), **c)** the VDFLL algorithm (in blue) and **d)** the total number of locked satellites during the car trajectory.

Moreover, a position error inflation for the VDFLL architecture based on the statistics given in Table 2 up to 75th epoch can be observed. This is due to the inclusion of the measurements coming from severely multipath affected satellite channels that are fed in the measurement innovation step of the VDFLL EKF estimation process. Whereas the proposed VDFLL algorithm benefits in terms of low positioning error and PVT solution, stability can be clearly seen from the 75th epoch up to the car trajectory end. The positioning divergence exhibited for the two scalar tracking architectures after the 75th epoch is due to the sudden changes of the number of locked satellites that in the KF domain is translated into less pseudoranges and Doppler measurements fed to the navigation module. On the other side, VDFLLs higher error statistics from the start of the car movement up to the 75th epoch are related to the inter-channel error coupling through its measurement innovation vector and NCO update process. However, the vectorized architecture exhibits a position stability in the final epochs. This comes from the fact that observations from all the satellites in view (not locked as for the scalar counterpart) are fed to the EKF estimation filter and properly de-weighted from its observation covariance matrix.

The performance analysis in the signal level for one of the seven tracked satellites, namely GPS PRN 12, in terms of code delay and Doppler frequency estimation errors is illustrated in Figure 8 and 9. The code delay and Doppler frequency estimation statistics in terms of their mean value and standard deviation for the scalar and vectorized architectures are summarized in Table 3. It must be noted that the channel level analysis is identical for two scalar tracking configurations since their only difference relies on the different position update rate.

A marked degradation of the vectorized architecture concerning the code tracking mean and standard deviation values can be easily noticed. The likely reason for this behavior is linked to the inclusion in the measurement innovation vector of the observations coming from a satellite channel under only NLOS reception condition. The consequence is inter-channel error propagation through the common EKF estimation filter and the estimation update based on the forward position/velocity projection in the vectorized architecture.

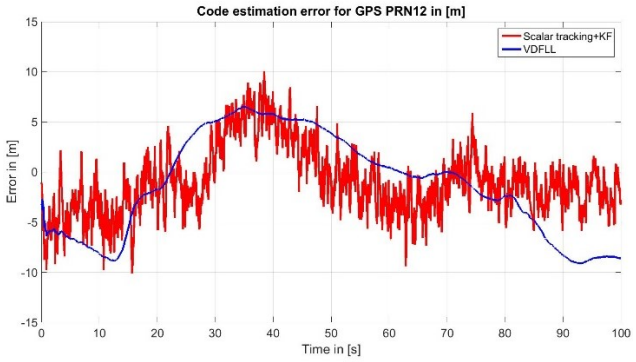

Figure 8. Code delay estimation error (in m) for the scalar tracking (in red) and VDFLL algorithm (in blue) of GPS PRN 12 for the dynamic user under multipath conditions.

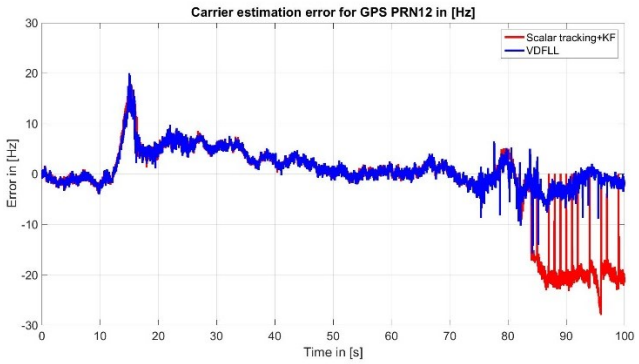

Figure 9. Carrier delay estimation error (in Hz) for the scalar tracking (in red) and VDFLL algorithm (in blue) of GPS PRN 12 for the dynamic user under multipath conditions.

Table 3. Code delay and Doppler frequency estimation statistics for the scalar tracking + KF position module and the proposed VDFLL technique.

	Scalar + KF		VDFLL	
	E[]	**Std[]**	**E[]**	**Std[]**
Code estimation error (m)	-0.97	4.11	-1.24	5.03
Doppler freq. estimation error (Hz)	-1.56	8.67	1.17	3.44
Comment : E[] - mean value Std[] - standard deviation				

Concerning the Doppler frequency estimation, the VDFLL algorithm outperforms the scalar tracking counterpart since the user dynamics are quite well predicted by the EKF filter since the measurement innovation process and state update is conducted at a very high rate of 50 Hz. Moreover in the last measurement epochs, where the scalar tracking mechanism fails to cope with the Doppler frequency estimation, the VDFLL tracking robustness rises into the play due to the inter-channel aiding never losing the signal lock.

CONCLUSIONS AND FUTURE WORK

In this paper, a vector delay/frequency-locked loop (VDFLL) architecture for a dual constellation L1/E1 GPS/Galileo receiver is proposed. After the mathematical description of the EKF filter's prediction and observation model, a detailed performance comparison in the position and tracking domain between the scalar tracking + KF positioning operating at two different rates (1 and 50 Hz) and VDFLL configuration was assessed under simulated multipath reception conditions using the DLR urban channel model. The results for the dynamic scenario showed that contrary to the conventional tracking, the L1/E1 VDFLL loop is able to provide a stable positioning solution within minimal error bounds even with a reduced number of satellites in view and in harsh signal fading conditions. Moreover, neither signals loss of lock conditions, nor reacquisition process is performed by the vectorized loop under high user dynamics or signal fading conditions. The likely reason for this behavior is linked to the inter-channel aiding through the update process based on the forward position/velocity projection in the vectorized architecture. However, in high number of observations scenario, there is no real gain of employing the VDFLL architecture and instead only an increased update rate of the EKF filter in the scalar tracking configuration is sufficient. Moreover, an optimization of the VDFLL algorithm shall be used based on a trade-off between keeping the corrupted measurements or their exclusion prior to the navigation module.

Future work will proceed on three fronts. First, the detailed performance analysis concerning the position and tracking accuracy will be extended to another vectorized architecture including a L1/E1 EKF estimation block per tracked channel with the vectorized navigation filter as already decribed above. Secondly, the VDFLL algorithm will be implemented through the use of Unscented Kalman Filter (UKF) that removes the state and observation errors Gaussian distribution constraint. Last but not least, the vectorized architecture will be extended to the carrier phase estimation in order to fully accomplish the positioning and tracking capability of vector tracking in signal-constrained environment.

ACKNOWLEDGMENTS

This work was financially supported by EU FP7 Marie Curie Initial Training Network MULTI-POS (Multi-technology Positioning Professionals) under grant nr. 316528.

REFERENCES

[1] Paul D. Groves, "Principles of GNSS, Inertial, and Multisensor Integrated Navigation Systems", *Artech House, 2008. Hardcover. 518 pages*.

[2] J. J. Spilker Jr., "Fundamentals of signal tracking theory," in *Global Positioning System: Theory and Applications, Volume 1, Chapter 7, ser. Progress in Astronautics and Aeronautics*, Washington DC, 1996.

[3] Pany T, Kaniuth R, Eissfeller B., "Deep Integration of Navigation Solution and Signal Processing" *Proc. ION-ITM-2005*, Long Beach, California, pp 1095 – 1102.

[4] Kaniuth R, Eissfeller B., "Deep Integration of Navigation Solution and Signal Processing" Proc. ION-ITM-2005, Long Beach, California, pp 1095 – 1102.

[5] Lashley, M., Bevly, D.M., Hung, J.Y., "A Valid Comparison of Vector and Scalar Tracking Loops," *Proceedings of IEEE/ION PLANS 2010*, Indian Wells, CA, May 2010, pp. 464-474.

[6] Elliott D. Kaplan, Christopher J. Hegarty, "Understanding GPS: Principles and Application," 2nd edition, Artech House, 2006

[7] X. Tang, G. Falco, E. Falletti and L. Lo Presti, "Theoretical Analysis and Tuning Criteria of the Kalman Filter-based Tracking Loop", *GPS Solutions 2014*, DOI: 10.1007/s10291-014-0408-2

[8] F. Sousa and F. Nunes, "Performance analysis of a VDFLL GNSS receiver architecture under ionospheric scintillation and multipath conditions,"in *Proceedings of the 2014 IEEE/ION Position, Location, and Navigation Symposium*, Monterey, CA, May 2014, pp. 602–611.

[9] Seco-Granados, G., Lopez-Salcedo, J.A., Jimenez-Banos, D., Lopez-Risueno, G.: Challenges in Indoor Global Navigation Satellite Systems, IEEE Signal Processing Magazine, March 2012, pp. 108-131.

[10] DLR, "Implementation of the Land Mobile Satellite Channel Model - Software Usage." 2007.

[11] DLR, "Land Mobile Satellite Channel Model - Interface Control Document." 2008.